RESERVOIR ENGINEERING FOR CO_2 STORAGE

FUNDAMENTAL & PRACTICAL ASPECTS

MEHDI ZEIDOUNI

PB
PENNWELL
BOOKS

Contents

Preface

This book is the result of countless hours of my effort to understand, develop, and apply various modeling tools to geologic CO_2 storage (GCS) projects. It is a publication I wish I had when I first started working on GCS at the University of Calgary in 2006. The book unifies diverse modeling approaches and presents them in a simple and comprehensive manner.

In this book, I strive to present the modeling of CO_2 storage in the subsurface considering the structure presented in Petroleum Engineering (PetE) curricula. In the early years of its development, CO_2 storage modeling efforts were mostly led by researchers with non-PetE backgrounds including physics, mathematics, and hydrogeology. As someone with all degrees in PetE: BSc from Abadan Institute of Technology (Petroleum University of Technology), Iran; MSc from Delft University of Technology, The Netherlands; and PhD from the University of Calgary, Canada, I was challenged with understanding the presented materials and relating them to the PetE literature. In writing this book, my intent is to make those materials readily available for readers with a PetE background or interest. Therefore, this book should be most useful to petroleum engineers and petroleum engineering undergraduate or graduate students who would like to learn GCS in petroleum engineering terminology.

Here is an overview of the materials in this book:

In Chapter 1, we cover the main drivers of GCS as a method to cut CO_2 atmospheric emissions, the main challenges to be addressed in GCS, the main options available for GCS, and the modeling challenges specific to GCS. In addition, CO_2 phase diagram is presented, and the CO_2 pressure and temperature conditions at the injection wells along with depth ranges for target formations are discussed. The importance of CO_2-brine mutual dissolution in saline aquifer or depleted reservoirs is then explained. The chapter ends with presenting the two main modeling approaches that can capture the physics of CO_2-brine displacement. These two modeling approaches are the fractional flow model and the interface model, which are presented in Chapters 2 and 3, respectively.

In Chapter 2, the concepts and theoretical background required to model the CO_2-brine displacement using the fractional flow theory are introduced. We start with disregarding the mutual dissolution between CO_2 and brine, for simplicity. The effect of CO_2-brine mutual dissolution will then be accounted for in the next

sections. Application of the model is presented for saline aquifers and depleted reservoirs as storage formations.

Chapter 3 presents the interface model, also known as the vertical equilibrium model. The model assumes a sharp interface separating CO_2 from other reservoir fluids. For low gravity numbers, the model results in a simple closed-form analytical solution to determine the interface. However, gravity numbers are generally high, requiring semi-analytical or numerical solutions which are also presented in this chapter. Again, example problems are provided to show the application of the model to CO_2 injection dynamics in saline aquifers and depleted reservoirs.

In Chapter 4, various models to estimate the overpressure during CO_2 injection are presented. The models are based on the assumption of various conditions on the external reservoir boundary, namely infinite-acting, open, and closed, while considering CO_2 distribution either based on a fractional flow model or interface model. Application of the estimated overpressure for calculation of the Area of Review is demonstrated. In addition, the concept of storage efficiency is introduced along with its sensitivity to the reservoir degree of closeness.

Chapter 5 provides an overview of the five main trapping mechanisms responsible for reducing the mobility of injected CO_2 in the subsurface. The mechanisms are structural and stratigraphic trapping, capillary trapping, residual trapping, mineral (geochemical) trapping, and dissolution trapping.

Chapter 6 focuses on GCS monitoring and verification. Among various monitoring approaches, pressure and temperature monitoring are covered in this chapter. The significance of monitoring pressure and temperature is introduced. Next, the different possibilities for acquiring and analyzing these data are presented. Concluding remarks and major remaining gaps are presented in Chapter 7.

The mathematical modeling tools are also presented in the form of hands-on MS Excel implementation tutorials to show the model application steps and usefulness. With this approach, I follow in the footsteps of my great teacher — Prof. Hans Bruining— who was the first to show me the effectiveness of using MS Excel in teaching complex mathematical models. I highly recommend that readers do the Excel exercises (presented in the book's appendices) to deepen their learning.

The book also includes True/False and short-answer questions intended to improve the reader's engagement and learning. I strongly encourage readers to answer these questions before continuing to read.

I hope this book proves useful. I welcome comments and suggestions for improvements to be implemented in future editions.

Mehdi Zeidouni
Baton Rouge, Louisiana

1

INTRODUCTION

Background

The increasing atmospheric concentration of some gases including carbon dioxide (CO_2) is recognized as a key driver of global temperature rise due to the "greenhouse effect." As the name suggests, this effect can be understood by analogy to a greenhouse. In a greenhouse exposed to sunlight, visible light passes through the glass ceiling, and gets absorbed by the ground and existing materials inside the greenhouse, warming them. These warm surfaces then emit energy as infrared radiation. Unlike visible light, infrared radiation cannot easily escape through the glass. Instead, it is absorbed and reflected back, raising the greenhouse's internal temperature.

In concept, the earth's atmosphere acts in the same way (Figure 1.1). Solar radiation enters the atmosphere, gets absorbed by the earth's surface, and warms it up. The warmed surface then emits energy primarily as infrared radiation. The emitted infrared radiation interacts with so-called greenhouse gases such as CO_2 and methane. These gases absorb the infrared radiation and re-emit it in all directions, including back toward the Earth's surface. This process slows the escape of heat into space, leading to an increase in atmospheric and surface temperatures.

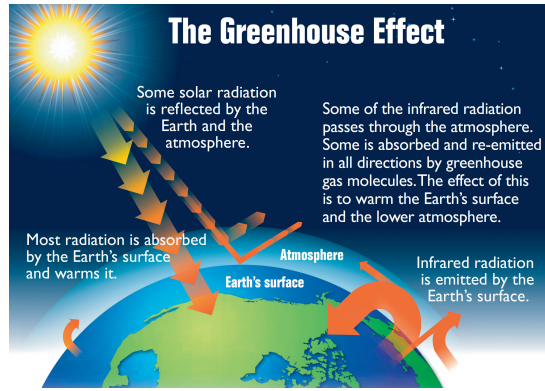

Figure 1.1. Schematic showing how greenhouse gases affect the atmospheric temperature. Wikimedia Commons. (Sep 29, 2024)

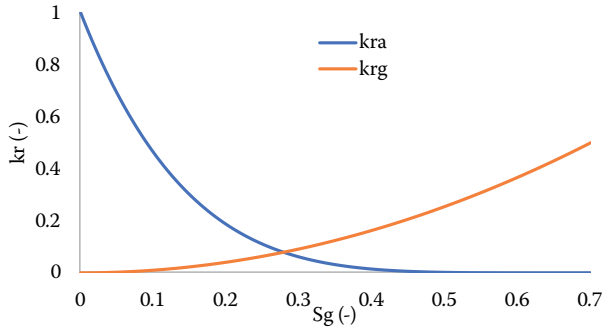

Figure 2.1. Relative permeability curves for the gaseous and aqueous phases.

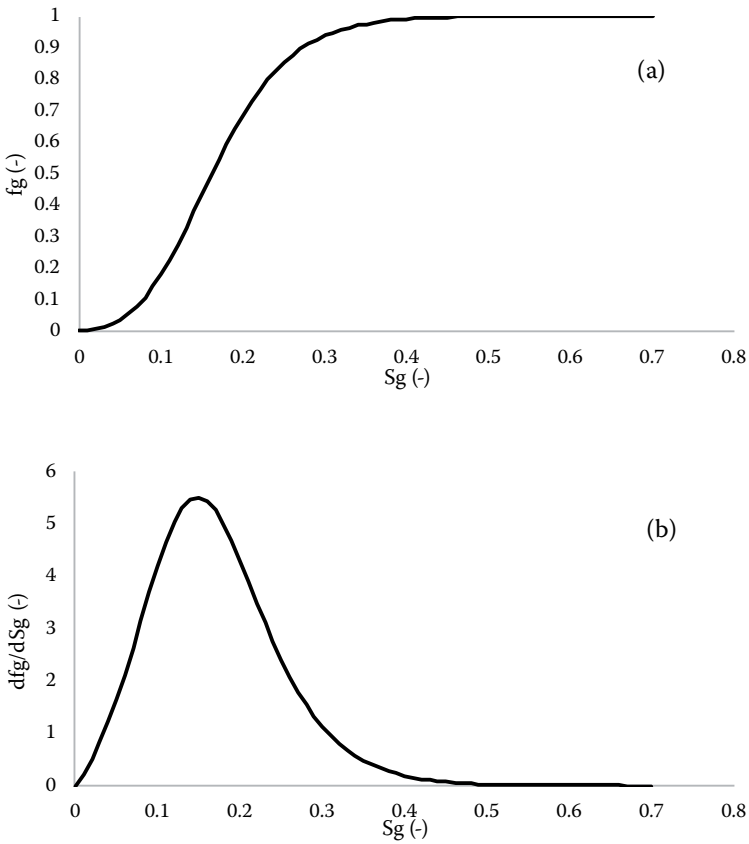

Figure 2.2. (a) The gaseous fractional flow curve, and (b) its derivative with respect to gaseous phase saturation.

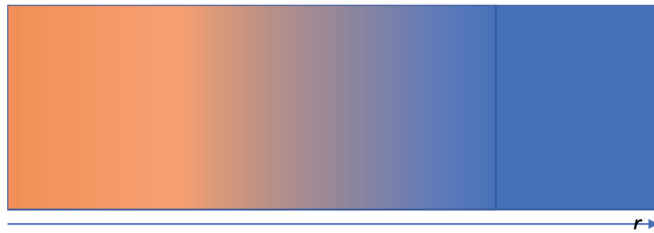

Figure 2.6. The saturation distribution according to the BL model. The blue indicates water, while orange shows the CO_2 gas phase. Notice that the saturation of CO_2 changes gradually within the CO_2 region (shown by transitioning from dark orange to light orange). However, there is an abrupt drop in CO_2 saturation at the front representing the shock.

Based on Eq. 2.10, and considering the fractional flow derivative at the shock $\left(\left.\frac{df_g}{dS_g}\right|_{S_g^f}\right)$, we can write:

$$\frac{r_{max}^2}{t} = \frac{q_t}{\pi h \phi}\left.\frac{df_g}{dS_g}\right|_{S_g^f} \tag{2.17}$$

where

r_{max} is the shock radius, which is the maximum extent of the CO_2 plume.

Rearranging this equation, we obtain:

$$\frac{q_t t}{\pi r_{max}^2 h \phi} = \frac{1}{\left.\frac{df_g}{dS_g}\right|_{S_g^f}} \tag{2.18}$$

The numerator on the left-hand side (LHS) of this equation is the cumulative volume of CO_2 injected. The denominator of the LHS is total pore space of the aquifer volume accessed by CO_2.

Therefore, the LHS is simply the average gas saturation within the CO_2 plume, i.e.,

$$\bar{S}_g = \frac{1}{\left.\frac{df_g}{dS_g}\right|_{S_g^f}} \tag{2.19}$$

When looking at Figure 2.4, this equation can be graphically interpreted. Extending the solid blue line to intersect the vertical axis results in the red circle shown in Figure 2.4. The x- and y-coordinates of the red circle are then $S_{g,intersect}$ and 1, respectively. Then, we can write:

Solution

a)

$$\frac{1}{\rho_g}=\frac{y_C}{\rho_C}+\frac{y_w}{\rho_w}=\frac{0.98}{11}+\frac{0.025}{58}\rightarrow \rho_g=11.18$$

$$\frac{1}{\rho_a}=\frac{x_C}{\rho_C}+\frac{x_w}{\rho_w}=\frac{0.025}{11}+\frac{0.975}{58}\rightarrow \rho_a=52.4$$

b)

$$S_g^I=f_g^I=\frac{\rho_a x_c}{\rho_a x_c-\rho_g y_c}=\frac{52.4\times 0.025}{52.4\times 0.025-11.18\times 0.98}=-0.1358$$

$$S_g^J=f_g^J=\frac{\rho_C-\rho_a x_C}{\rho_g y_C-\rho_a x_C}=\frac{11-52.4\times 0.025}{11.18\times 0.98-52.4\times 0.025}=1.0044$$

c) Drawing the tangent line from points I and J will give the dissolution and vaporization saturations, respectively:

$$S_g^d=0.340 \text{ and } S_g^v=0.633$$

d)

$$r_{max}=\sqrt{\frac{q_t t}{\pi h\phi}\left.\frac{df_g}{dS_g}\right|_{S_g^d}}=\sqrt{\frac{0.015\times 180\times 86400}{\pi\times 40\times 0.35}\times 2.06}=104.3 \text{ m}$$

$$r_{dry}=\sqrt{\frac{q_t t}{\pi h\phi}\left.\frac{df_g}{dS_g}\right|_{S_g^v}}=\sqrt{\frac{0.015\times 180\times 86400}{\pi\times 40\times 0.35}\times 0.013}=8.3 \text{ m}$$

e)

$$\bar{S}_g=\frac{S_g^d\left.\frac{df_g}{dS_g}\right|_{S_g^d}-S_g^v\left.\frac{df_g}{dS_g}\right|_{S_g^v}-\left(f_g^d-f_g^v\right)}{\left.\frac{df_g}{dS_g}\right|_{S_g^d}-\left.\frac{df_g}{dS_g}\right|_{S_g^v}}$$

$$=\frac{0.34\times 2.06-0.633\times 0.013-(0.843-1)}{2.06-0.013}=0.41$$

f)

$$\text{Dissolved } CO_2 \text{ fraction}=\left(\left.\frac{df_g}{dS_g}\right|_{S_g^d}-\left.\frac{df_g}{dS_g}\right|_{S_g^v}\right)\frac{\left(1-\bar{S}_g\right)\rho_a x_c}{\rho_c}$$

$$=(2.06-0.013)\times(1-0.41)\times\left(52.4\times\frac{0.025}{11.18}\right)=0.14$$

Solution

(a) First, let the methane and CO_2 be two different phases, considering their different densities. Also, ignore the irreducible water saturation and assign the effective porosity to be $\phi_{eff} = \phi(1 - S_{wi}) = 0.25 \times (1 - 0.3) = 0.175$. The effective porosity represents the pore volume, which is filled by either CO_2 or methane. When using the equations presented in this chapter, porosity should be replaced by ϕ_{eff} and irreducible water saturation should be considered zero.

Given that CO_2 density is higher than methane, CO_2 will be below the interface and methane is above it. All effective pore space below the interface will be taken by CO_2, and all that above the interface is taken by methane. Let h_a denote the CO_2 column below the interface and h_g be the methane interval above the interface. The following equation is still valid:

$$h_{aD} = \frac{\sqrt{\frac{2M}{\chi}} - M}{1 - M}$$

However, in this case, $h_{aD}(\chi_{max}) = 0$ and $h_{aD}(\chi_{min}) = 1$. As such, $\chi_{max} = 2/M$ and $\chi_{min} = 2M$. The interface is therefore given by:

$$h_{aD} = \begin{cases} 1, & \chi \le 2M \\ \dfrac{M - \sqrt{\frac{2M}{\chi}}}{M - 1}, & 2M < \chi < 2/M \\ 0, & \chi \ge 2/M \end{cases}$$

The mobility ratio is:

$$M = \frac{1/0.05}{1/0.025} = 0.5$$

Therefore, $\chi_{max} = \dfrac{2}{0.5} = 4$. Then,

$$r_{max} = \sqrt{\frac{\chi_{max} q_t t}{2\pi h \phi_{eff}}} = \sqrt{\frac{4 \times 0.01 \times 100 \times 86400}{2 \times 3.14 \times 30 \times 0.175}} = 102.4\,m$$

(b)

$$\bar{S}_g = \frac{q_t t}{\pi h \phi_{eff} r_{max}^2} = \frac{2}{\chi_{max}} = \frac{2}{2/M} = M = 0.5$$